Purdue University
Purdue e-Pubs

Publications of the Ray W. Herrick Laboratories | School of Mechanical Engineering

9-2003

Holographic Visualization of Noise Emissions from a Small Ducted Fan

Moohyung Lee
Purdue University

J Stuart Bolton
Purdue University, bolton@purdue.edu

Luc Mongeau
Purdue University

Follow this and additional works at: https://docs.lib.purdue.edu/herrick

Lee, Moohyung; Bolton, J Stuart; and Mongeau, Luc, "Holographic Visualization of Noise Emissions from a Small Ducted Fan" (2003). *Publications of the Ray W. Herrick Laboratories.* Paper 220.
https://docs.lib.purdue.edu/herrick/220

This document has been made available through Purdue e-Pubs, a service of the Purdue University Libraries.
Please contact epubs@purdue.edu for additional information.

Fan Noise 2003

HOLOGRAPHIC VISUALIZATION OF NOISE EMISSIONS FROM A SMALL DUCTED FAN

Moohyung LEE, J. Stuart BOLTON, Luc MONGEAU

Ray W. Herrick Laboratories, School of Mechanical Engineering, Purdue University, 140 S. Intramural Drive, West Lafayette, IN 47907-2031, U.S.A.

SUMMARY

Cylindrical Nearfield Acoustical Holography (NAH) based on a multi-scan, cross-spectral measurement was used to visualize the sound field of a ducted fan, and the ability of this procedure to quantify source modification effects is illustrated here.

INTRODUCTION

Up to now, there have been many experimental investigations aimed at understanding the sound generation and radiation characteristics of fan noise sources. Sound intensity measurements have been used for source location and Particle Image Velocity (PIV) measurements have been used in an attempt to correlate flow fields with sound radiation. At the same time, many array measurement techniques such as the acoustic mirror, the acoustic telescope and polar correlation were developed to identify sources within high speed jet turbofan engines. These techniques that are based on farfield measurements. In contrast NAH is based on measurements made in a source's nearfield, and can be used to visualize the sound field in a three-dimensional space by projecting the sound field measured on a two-dimensional surface to any surfaces of interest with almost unlimited spatial resolution [1].

In the case of a noise source that comprises multiple uncorrelated sub-sources, multiple reference microphones are required in order to enable both a scanning measurement and the decomposition of the field into incoherent partial fields [2]. In the past, the NAH procedure for the visualization of multiple incoherent sources has been implemented using two different approaches to partial field decomposition: the virtual coherence method and the partial coherence method [3]. Although those methods differ in the way the sound field is decomposed, the composite holographic projections that result are the same in either case under ideal circumstances.

Since NAH was first proposed by Williams and others in the 1980's, it has been used to study many sound radiation problems. However, most applications were focused on sound radiation from vibrating structures. In the present study, the NAH procedure based on the use of the virtual coherence method was applied to visualize the sound field of an aeroacoustic source (a small ducted fan). The frequency range of interest in this test was below 400 Hz, in which range a small fan is usually considered a compact dipole source.

THEORETICAL BACKGROUND

Partial field decomposition by using multiple references

Consider the case of a noise source that consists of multiple uncorrelated sub-sources. If it was possible to measure the contribution of each incoherent source separately, each partial field could be projected independently by using NAH: the partial fields could then be added on an energy basis to reconstruct the total field. However this approach is not possible in practical cases since it is not usually possible to measure the partial fields individually. Alternatively, a cross-spectral procedure based on using a set of reference signals can be implemented. The latter signals can be used to decompose the composite sound field into a set of linearly independent, partial fields.

Here the virtual coherence method was used to perform the partial field decomposition. Singular Value Decomposition (SVD) plays a crucial role in this method since it can be used both to diagonalize the reference cross-spectral matrix, $\mathbf{C}_{rr}$, and to determine the number of references required to describe the sound field: i.e.,

$$\mathbf{C}_{\mathrm{rr}} = \mathrm{E}\left[\mathbf{r}^{*}\mathbf{r}^{\mathrm{T}}\right] \xrightarrow{SVD} \mathbf{U}\boldsymbol{\Sigma}\mathbf{V}^{\mathrm{H}} = \mathbf{U}\boldsymbol{\Sigma}\mathbf{U}^{\mathrm{H}}, \tag{1}$$

where $\mathbf{r} = [r_1 \cdots r_N]^{\mathrm{T}}$ is a reference signal vector, N is the number of references, E denotes ensemble average, $\boldsymbol{\Sigma}$ is a diagonal matrix composed of the singular values, σ_i', and $\mathbf{U}$ and $\mathbf{V}$ are unitary matrices that are composed of the left and right singular vectors, respectively. Since $\mathbf{C}_{rr}$ is a semi-positive definite, Hermitian matrix, $\mathbf{U}$ and $\mathbf{V}$ are identical in this case. To perform an effective decomposition, it is required that the number of references should be equal to or larger than the number of singular values greater than the background noise level [4]. Note that, in practical cases, the number of references determined by SVD does not exactly correspond to the number of the actual uncorrelated sources creating the total sound field. Since measured spectra may be in error, especially due to bias errors introduced by Finite Discrete Fourier Transform (DFT) operations, additional artificial sources may be introduced. That is, the number of singular values greater than the background noise level may be greater than the number of the actual sources [5].

In the virtual coherence method, the decomposed partial fields, $\hat{\mathbf{P}}$, can be calculated in the following way:

$$\hat{\mathbf{P}} = \hat{\mathbf{H}}_{rp}^{\mathrm{T}}\boldsymbol{\Sigma}^{1/2} = \mathbf{H}_{rp}^{\mathrm{T}}\mathbf{U}^{*}\boldsymbol{\Sigma}^{1/2} = \mathbf{C}_{rp}^{\mathrm{T}}\mathbf{U}^{*}\boldsymbol{\Sigma}^{-1/2}, \tag{2}$$

where $\mathbf{H}_{rp}$ is the transfer matrix that relates the reference signals and the measured field signals on the hologram surface, $\mathbf{C}_{rp}$ is a cross-spectral matrix between the reference and field microphone signals, and the i th column vector of $\hat{\mathbf{P}}$ represents the i th partial field. Note that the decomposed partial fields are subject to the condition $\mathbf{C}_{pp} = \hat{\mathbf{P}}^{*}\hat{\mathbf{P}}^{\mathrm{T}}$.

The sufficiency of the reference set determined by applying SVD can be verified by calculating the virtual coherence, γ_{ij}^2, at each frequency of interest: i.e.,

$$\gamma_{ij}^2 = \left|\hat{r}_j^{*} p_i\right|^2 \Big/ (p_i^{*} p_i)(\hat{r}_j^{*}\hat{r}_j) \ , \tag{3}$$

where $\mathbf{p} = [p_1 \cdots p_M]^{\mathrm{T}}$ is a pressure vector measured on the hologram surface, M is the number of measurement points, $\hat{\mathbf{r}} = [\hat{r}_1 \cdots \hat{r}_N]^{\mathrm{T}}$ is the virtual reference vector defined by

$\hat{\mathbf{r}} = \mathbf{U}^{\mathrm{T}}\mathbf{r}$, i denotes the ith measurement point, and j denotes the jth partial field. The sum of the virtual coherences, $\sum_{j=1}^{N}\gamma_{ij}^2$, indicates how well a subset of virtual references describes the sound field: if its value is nearly unity, the reference set is sufficient.

When the sound field is measured by scanning a sub-array over a number of patches in sequence, the reference cross-spectral matrix may vary from scan-to-scan owing to the slight non-stationarity that is characteristic of aeroacoustic sources. In this case, the partial fields calculated by direct application of Eq. (2) may be corrupted by spatial noise in the shape of the sub-array. In contrast, the transfer matrix, $\mathbf{H}_{rp}$, calculated for each patch is likely to be independent of source levels since it represents amplitude and phase information *relative* to the sources. When $\mathbf{H}_{rp}$ is independent of source level, the effects of source non-stationarity can be compensated for by modifying Eq. (2), and using the relation $\mathbf{H}_{rp} = \mathbf{C}_{rr}^{-1}\mathbf{C}_{rp}$ to form [6]

$$\hat{\mathbf{P}} = \mathbf{H}_{rp\,(\mathrm{scan})}^{\mathrm{T}}\mathbf{U}_{(\mathrm{avg})}^{*}\boldsymbol{\Sigma}_{(\mathrm{avg})}^{1/2} = \left(\mathbf{C}_{rr\,(\mathrm{scan})}^{-1}\mathbf{C}_{rp\,(\mathrm{scan})}\right)^{\mathrm{T}}\mathbf{U}_{(\mathrm{avg})}^{*}\boldsymbol{\Sigma}_{(\mathrm{avg})}^{1/2}, \tag{4}$$

where the subscripts (scan) and (avg) denote estimates calculated during each scan and estimates averaged over all scans, respectively. The partial fields calculated using Eq. (4) can be used as input to the NAH equations presented in the following section.

Cylindrical Nearfield Acoustical Holography (NAH)

When implementing exterior, cylindrical NAH in an anechoic space, the homogeneous, time-independent Helmholtz equation in cylindrical coordinates for the acoustic pressure, $\hat{p}(r,\phi,z)$, is solved by the method of separation of variables, and the pressure field can be expressed in terms of cylindrical modal functions: i.e.,

$$\hat{p}(r,\phi,z) = \sum_{n=-\infty}^{\infty} e^{in\phi}\,\frac{1}{2\pi}\int_{-\infty}^{\infty} A_n(k_z,\omega)H_n^{(1)}(k_r r)e^{ik_z z}dk_z\ , \tag{5}$$

where $k_r = \sqrt{k^2 - k_z^2}$, k_r and k_z are the radial and axial wave number, respectively, $k = \omega/c$, $A_n(k_z,\omega)H_n^{(1)}(k_r r)$ is the two-dimensional Fourier transform, $\hat{P}_n(r,k_z)$, of $\hat{p}(r,\phi,z)$ (i.e., the *helical wave spectrum*), and $H_n^{(1)}$ is the Hankel function of the first kind. Once the wave number spectrum on the cylindrical hologram surface is known, the acoustical properties (i.e., pressure, particle velocity and intensity) can be calculated in a three-dimensional volume by multiplying the wave number spectrum by an appropriate propagator and then taking an inverse Fourier transform to obtain [1]:

$$\hat{p}(r,\phi,z) = \sum_{n=-\infty}^{\infty} e^{in\phi}\,\frac{1}{2\pi}\int_{-\infty}^{\infty}\hat{P}_n(r_h,k_z)\frac{H_n^{(1)}(k_r r)}{H_n^{(1)}(k_r r_h)}e^{ik_z z}dk_z\ , \tag{6}$$

$$\hat{w}(r,\phi,z) = \sum_{n=-\infty}^{\infty} e^{in\phi}\,\frac{1}{2\pi}\int_{-\infty}^{\infty}\hat{P}_n(r_h,k_z)\frac{-ik_r}{\rho ck}\frac{H_n^{(1)'}(k_r r)}{H_n^{(1)}(k_r r_h)}e^{ik_z z}dk_z\ , \tag{7}$$

where $\hat{w}$ is the radial particle velocity, r is the radius of the surface of interest, r_h is the radius of the hologram surface, ρ is the ambient density, and $\{\cdot\}'$ denotes a derivative with respect to the argument.

Due to the existence of rapidly decaying radial components associated with subsonic axial components, backward projection towards the source is an ill-posed problem. Typically, noisy high wave number components are amplified when projected back towards the source. As a result, reconstruction quality can be poor without additional processing. To prevent this problem, a regularization process is required. Here, an improved Tikhonov Regularization Theorem and the Mozorov Discrepancy Principle were used for *k*-space filtering based on a knowledge of the variance of the noise components [7].

Considerations related to the measurement of aeroacoustic sources

Aeroacoustic sources are usually accompanied by a mean flow which may impinge on either the field or reference microphones or both. When microphones are exposed to flow, the measured data contains the self-noise generated by the interaction of the flow and the microphone as well as the desired signal. This problem can be addressed by the proper placement of the various microphones: first, the reference microphones should be placed out of the flow, and secondly, the reference microphones should not sense any flow noise generated by the interaction of the flow with the field microphones [8].

When both reference and field microphones are placed in the flow, the measured reference signal, $\mathbf{r}_{\text{total}}$, and the field microphone signal, $\mathbf{p}_{\text{total}}$, can be expressed as,

$$\mathbf{r}_{\text{total}} = \mathbf{r}_s + \mathbf{r}_{sr} + \mathbf{r}_{sf}\,, \tag{8}$$

$$\mathbf{p}_{\text{total}} = \mathbf{p}_s + \mathbf{p}_{sr} + \mathbf{p}_{sf}\,, \tag{9}$$

where the subscripts *s*, *sr*, and *sf* denote the signal from the actual source, the self-noise generated by flow over the references, and the self-noise generated by flow over the field microphones, respectively. It is assumed here that all sources are mutually uncorrelated. Based on Eqs. (8) and (9), the cross-spectra between the references, and between the references and the field microphones can be expressed as:

$$\mathbf{C}_{rr,\text{total}} = \mathbf{r}^*_{\text{total}}\mathbf{r}^{\text{T}}_{\text{total}} = \mathbf{r}^*_s\mathbf{r}^{\text{T}}_s + \mathbf{r}^*_{sr}\mathbf{r}^{\text{T}}_{sr} + \mathbf{r}^*_{sf}\mathbf{r}^{\text{T}}_{sf}\,, \tag{10}$$

$$\mathbf{C}_{rp,\text{total}} = \mathbf{r}^*_{\text{total}}\mathbf{p}^{\text{T}}_{\text{total}} = \mathbf{r}^*_s\mathbf{p}^{\text{T}}_s + \mathbf{r}^*_{sr}\mathbf{p}^{\text{T}}_{sr} + \mathbf{r}^*_{sf}\mathbf{p}^{\text{T}}_{sf}\,. \tag{11}$$

It is very important that the reference cross-spectra should not be corrupted by unwanted noise since the reference cross-spectra play a crucial role in the partial field decomposition. Since the self-noise is created locally, it is clear that $\mathbf{r}_{sf}$ and $\mathbf{p}_{sr}$ will be negligibly small as long as the reference and field microphones are not placed in close proximity. The off-diagonal components of the second term in Eq. (10), $\mathbf{r}^*_{sr}\mathbf{r}^{\text{T}}_{sr}$ (i.e., the cross-spectra between the references), are suppressed by spectral averaging, but the diagonal components (i.e., the reference self-noise auto-spectra) remain. To remove the latter terms, it is thus absolutely necessary that the self-noise generated by flow over the references should be negligibly small compared to the actual source signal. The best way to satisfy the latter condition is simply to place the references out of the flow, in which case $\mathbf{r}_{sr}$ is equal to zero. Unless the flow speed over the field microphones is significant, the inequality $\left|\mathbf{r}^*_{sf}\mathbf{p}^{\text{T}}_{sf}\right| << \left|\mathbf{r}^*_s\mathbf{p}^{\text{T}}_s\right|$ should hold, thus making the third term in Eq. (11) negligible. Thus, in principle, the self-noise effect can be successfully removed from the measured cross-spectra so long as the self-

noise generated by flow over the reference microphones is negligibly small. Under these conditions, self-noise does not corrupt the holographic processing. However, the amplitudes of the diagonal components of $\mathbf{p}_{sf}^{*}\mathbf{p}_{sf}^{\mathrm{T}}$ (i.e., the auto-spectra of field microphone self-noise) are problematical. Those components do not affect the accuracy of the partial field decomposition, but cause the virtual coherence on the hologram surface to drop since $p_i^{*} p_i$ in Eq. (3) is overestimated. Therefore, when there is flow over the field microphones, care should be taken when interpreting the virtual coherence to determine whether or not one particular set of virtual references is sufficient.

EXPERIMENTAL APPRATUS

A cylindrical frame supporting an 8-by-8 array of measurement positions was constructed on a surface enclosing the source of interest (Fig. 1(a)). The measurement positions were separated by 39 cm in the *z*-direction (i.e., the axial direction) and 45 deg. in the ϕ-direction (i.e., the circumferential direction); the measurement radius was 50 cm, and the source was placed at the center of the cylindrical array. The measurements were performed using three reference microphones and four field microphones to scan the hologram surface in 16 steps, and both reference and field microphones were located out of the flow to minimize self-noise effects.

Holographic tests were first performed to visualize the sound radiation from the ducted fan shown in Fig. 1(b). The system was then altered to investigate the effect of two modifications on the radiation pattern: first, leaks were created (Fig. 1(b)), and secondly sound absorbing material was used to line the downstream duct section (Fig. 1(c)).

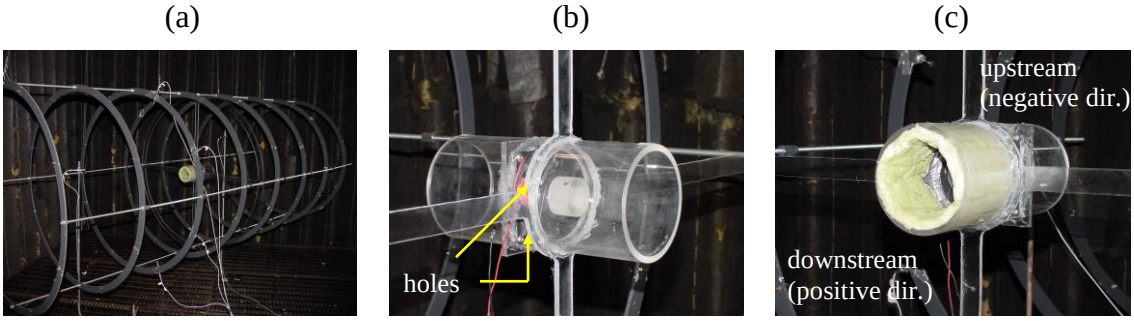

Figure 1: Experimental setup (a) measurement array (ducted fan located at the center of the frame) (b) locations of the holes in fan housing, (c) downstream fiber glass duct lining.

RESULTS

Since the fan used for these tests had five blades, the blade passing tone at five times the shaft rotation frequency was the largest component in the radiated sound field. Results in all three cases are shown at the blade passage tone (361 Hz) and for one broadband noise component (330 Hz).

First, the singular values of the reference cross-spectral matrix were examined to establish the number of references needed for the partial field decomposition: see Fig. 2. In all three cases, the levels of the third singular values at both frequencies dropped close to the background noise level. Therefore, the three references used for the measurements, in principle, were sufficient to describe the sound field.

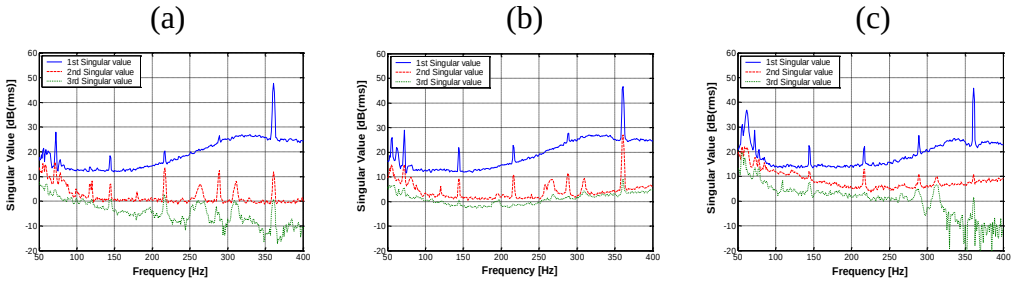

Figure 2: Singular values of $\mathbf{C}_{rr}$ *: (a) the first case, (b) the second case, (c) the third case.*

Secondly, the virtual coherences were used to verify that the number of virtual references determined by use of SVD was sufficient (subject to the restrictions described earlier). In all three cases, the virtual coherences calculated using one or two partial fields were nearly unity at both frequencies (Figs. 3 and 4). The virtual coherence results thus confirmed that the number of references was chosen appropriately. It was also concluded that the first partial field was the primary contributor to the total sound field except at the blade passing tone in the second case. Apparently, the introduction of the holes in the fan housing caused a second source mechanism to be significant.

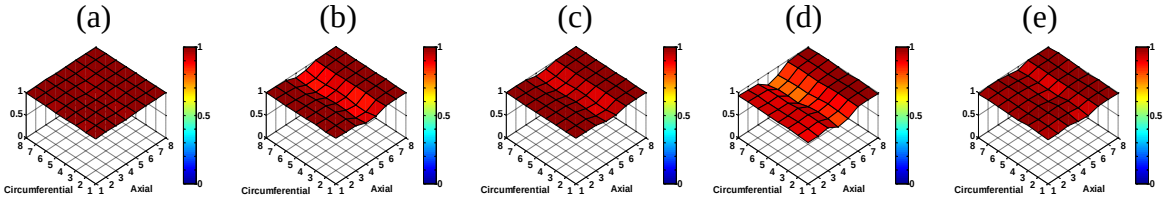

Figure 3: Virtual coherences at 330 Hz: (a) γ_{i1}^2 *for the first case, (b)* γ_{i1}^2 *for the second case, (c)* $\gamma_{i1}^2 + \gamma_{i2}^2$ *for the second case, (d)* γ_{i1}^2 *for the third case, (e)* $\gamma_{i1}^2 + \gamma_{i2}^2$ *for the third case.*

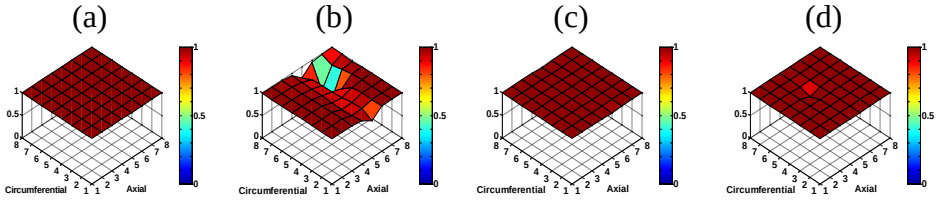

Figure 4: Virtual coherences at 361 Hz: (a) γ_{i1}^2 *for the first case, (b)* γ_{i1}^2 *for the second case, (c)* $\gamma_{i1}^2 + \gamma_{i2}^2$ *for the second case, (d)* γ_{i1}^2 *for the third case.*

Thirdly, the spatial distributions of the partial fields on the hologram surface were calculated by using NAH. In the first case, it was found that both the broadband noise and the blade passing tone exhibited a clear dipole-like directivity: i.e., the fields on the up- and downstream sides of the fan were 180 deg. out-of-phase (Figs. 5(a) and 6(a)). In the second case, the broadband noise still exhibited a dipole-like directivity (Fig. 5(b)) although there was a small contribution of the second source mechanism (Fig. 5(c)), but the radiation pattern at the blade passing tone was significantly changed by the effects of leakage (Figs. 6(b) and

(c)). It was found that leakage had a stronger effect on the blade passing tone than on the broadband noise. In the third case, a dipole-like directivity was preserved at both frequencies although a small amount of distortion was observed. In Fig. 7, the distinction between the two types of radiation patterns (i.e., dipole-like and directional radiation) can be seen clearly.

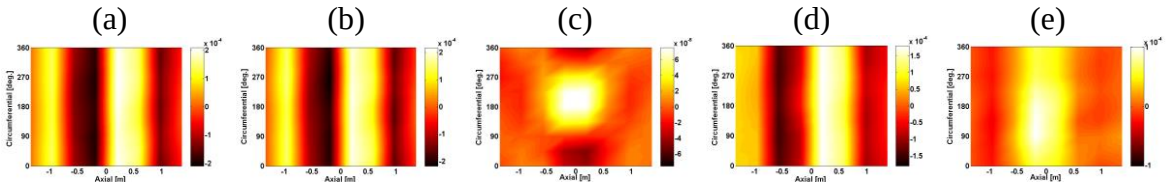

Figure 5: Partial fields at 330 Hz (real part plotted): (a) $\hat{\mathbf{p}}_1$ for the first case, (b) $\hat{\mathbf{p}}_1$ for the second case, (c) $\hat{\mathbf{p}}_2$ for the second case, (d) $\hat{\mathbf{p}}_1$ for the third case, (e) $\hat{\mathbf{p}}_2$ for the third case.

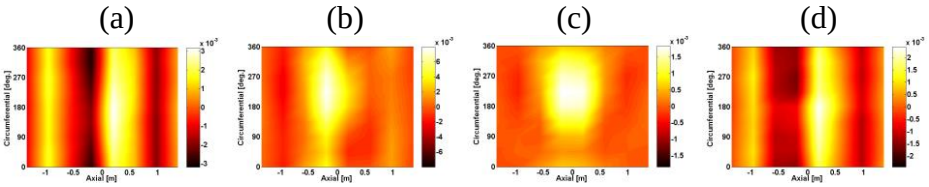

Figure 6: Real Partial fields at 361 Hz (real part plotted): (a) $\hat{\mathbf{p}}_1$ for the first case, (b) $\hat{\mathbf{p}}_1$ for the second case, (c) $\hat{\mathbf{p}}_2$ for the second case, (d) $\hat{\mathbf{p}}_1$ for the third case.

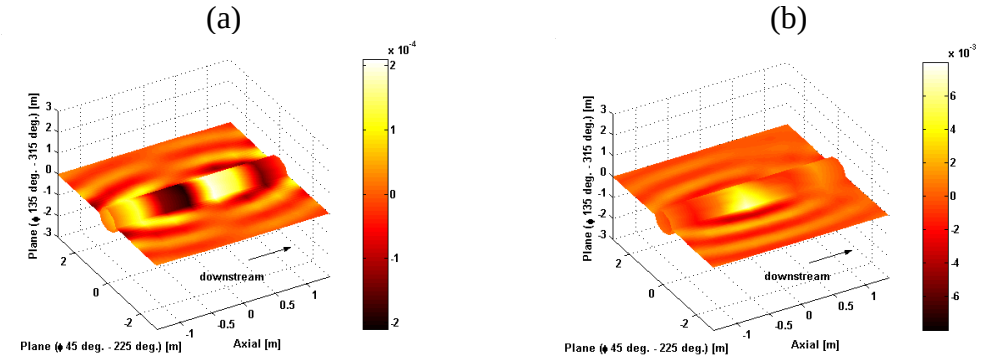

Figure 7: Three-dimensional reconstruction of the pressure field (real part of the first partial field plotted): (a) 330 Hz for the first case, (b) 361 Hz for the second case

Finally, the farfield directivities for several cases were calculated on the plane defined by $\phi = 45^\circ$ and 225°. In Fig. 8(a), the directivity pattern of the broadband noise component in the first case is compared with that of a theoretical dipole. The blade passing tone in the second case exhibited a main lobe extending in the negative-*z* direction (Fig. 8(b)). Figure 8(c) compares the directivity patterns of the blade passing tone in the first and third cases. The overall sound level decreased but increased slightly in the direction perpendicular to the dipole axis due to the effect of the lining. The downstream radiation is slightly reduced by comparison with the upstream radiation, presumably, because of the absorbent lining in the downstream duct section.

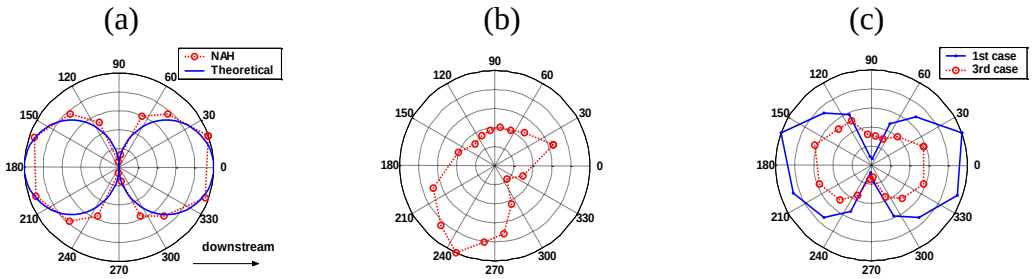

Figure 8: Directivity plots: (a) for the first case at 330 Hz (along with comparison to theoretical dipole directivity), (b) for the second case at 361 Hz, (c) for the third case at 361 Hz (along with comparison to the first case).

CONCLUSIONS

In this article, the application of cylindrical NAH procedures to aeroacoustic sources has been described. First, the procedures for determining the number of references required to describe the sound field with the help of SVD and virtual coherence analysis were described. The procedure for decomposing the sound field into the partial fields by using the virtual coherence method was outlined. After decomposition, each partial field can be projected to the reconstruction surface after appropriate regularization. By comparing the visualized sound fields corresponding to the various configurations, the ability of NAH to quantify the effect of noise source modification effects was demonstrated for the case of a ducted fan.

BIBLIOGRAPHY

[1] E. G. Williams - *Fourier Acoustics: Sound Radiation and Nearfield Acoustical Holography*. Academic Press, London, UK, **1999**.

[2] J. Hald - *STSF – A Unique Technique for Scan-based Near-Field Acoustic Holography without Restrictions on Coherence*. B&K Technical Review No. 1, **1988**.

[3] D. L. Hallman and J. S. Bolton - *A Comparison of Multi-Reference Nearfield Acoustical Holography Procedures*. Proceedings of NOISE-CON 94, p. 929-934, **1994**.

[4] S. H. Yoon and P. A. Nelson - *A Method for the Efficient Construction of Acoustic Pressure Cross-Spectral Matrices*. Journal of Sound and Vibration, 233(5), p. 897-920, **2000**.

[5] M. S. Kompella, P. Davies, R. J. Bernhard, and D. A. Ufford - *A Technique to Determine the Number of Incoherent Sources Contributing to the Response of a System*. Mechanical Systems and Signal Processing, 8(4), p. 363-380, **1994**.

[6] H.-S. Kwon, Y.-J. Kim, and J. S. Bolton - *Compensation for Source Non-Stationarity in Multi-Reference, Scan-Based Nearfield Acoustical Holography*. Journal of the Acoustical Society of America, 113, p. 360-368, **2003**.

[7] E. G. Williams - *Regularization Method for Near-Field Acoustical Holography*. Journal of the Acoustical Society of America, 110, p. 1976-1988, **2001**.

[8] M. Nakamura, T. Komine, M. Tsuchiya, and J. Hald - *Measurement of Aerodynamic Noise using STSF*. B&K application note, **1990**.